Structural investigation of a new cadmium coordination compound prepared by sonochemical process: crystal structure, Hirshfeld surface, thermal, TD-DFT and NBO analyses

A. Masoudiasl, M. Montazerozohori, S. Joohari, L. Taghizadeh, G. Mahmoudi, A. Assoud

PII: S1350-4177(18)30838-1
DOI: https://doi.org/10.1016/j.ultsonch.2018.11.024
Reference: ULTSON 4393

To appear in: *Ultrasonics Sonochemistry*

Received Date: 1 June 2018
Revised Date: 28 September 2018
Accepted Date: 25 November 2018

Please cite this article as: A. Masoudiasl, M. Montazerozohori, S. Joohari, L. Taghizadeh, G. Mahmoudi, A. Assoud, Structural investigation of a new cadmium coordination compound prepared by sonochemical process: crystal structure, Hirshfeld surface, thermal, TD-DFT and NBO analyses, *Ultrasonics Sonochemistry* (2018), doi: https://doi.org/10.1016/j.ultsonch.2018.11.024

Structural investigation of a new cadmium coordination compound prepared by sonochemical process: crystal structure, Hirshfeld surface, thermal, TD-DFT and NBO analyses

A. Masoudiasl[a], M. Montazerozohori [a*], S. Joohari[b], L. Taghizadeh[a], G. Mahmoudi[d], A. Assoud[c]

[a]Department of Chemistry, Yasouj University, Yasouj 75918-74831, Iran
[b]Department of Basic Sciences, Yasooj Branch, Islamic Azad University, Yasooj, Iran
[C]Department of Chemistry, University of Waterloo, Waterloo, Ontario, Canada, N2L 3G1.
[d]Department of Chemistry, Faculty of Science, University of Maragheh, P.O. Box 55181-83111, Maragheh, Iran
*Email address: mmzohory@yahoo.com

Abstract

A new nanostructured cadmium complex containing a tridentate Schiff base ligand was sonochemically synthesized and characterized by XRPD, FT/IR, NMR, and single crystal X-ray crystallography. Structural data showed that cadmium(II) ion is surrounded by three nitrogen atoms of Schiff base ligand and two iodide anions. The crystal packing was contained the intermolecular interactions such as C–H···O, C–H···I and π···π interactions organizing the self-assembly process. Hirshfeld surfaces and corresponding fingerprint plots have been used for investigation of the nature and proportion of interactions in the crystal packing. FT/IR, NMR and XRD data were in agreement with the X-ray structure and confirm the phase purity of the prepared sample. The molecular structure of the complex was optimized by density functional theory (DFT) calculation at the B3LYP/LANL2DZ level of theory and the results were compared with experimental ones. For more concise study of structure and spectral aspects of the complex, natural bond orbital (NBO) analysis and time-dependent density functional theory (TD-DFT) have been also performed. Thermal stability of the cadmium iodide complex was investigated by thermogravimetric analysis (TGA). Finally, cadmium oxide nanoparticles was prepared by direct calcination of $CdLI_2$ complex as a new precursor.

Introduction

The Schiff bases derived diethylenetriamine and aldehydes have attracted remarkable attention because of their interesting properties and the coordination potential of them [1-3]. Diethylenetriamine alone can be coordinated to metal in various forms. In simplest form, this compound is a tridentate ligand with three aminic nitrogen donors [4, 5]. One of the most common ligands based on diethylenetriamine are Schiff base ligands from bidentate to multidentate macrocyclic ligands [6-8]. Cadmium is an IIB element that prefers oxidation

state of 2+ with spherical d^{10} configuration in most of its compounds, and in its coordination compounds commonly accepts four to eight coordination numbers [9]. Cadmium Schiff base complexes based on diethylenetriamine may be interesting due to their structural properties [8,10,11].

Increasing energy consumption and related environmental problems are one of the most challenging human concerns. Therefore, the uses of energy-saving and environmentally friendly methods in the process of production and consumption of energy have an essential importance. In the synthetic chemistry, sonochemistry as a modern synthetic method is an environmentally friendly and energy saving technique for the synthesis of the coordination compounds [12-14]. This method is an effective alternative for common methods and its application is rapidly expending in coordination chemistry [15-18]. Chemical changes induced by sonochemical process occurs via acoustic cavitation (i.e., the formation, growth and instantaneously implosive collapse of the bubbles in liquid) leading to high pressures, intense local heating and very short lifetimes [19, 20]. Nanostructured compounds with interesting physical and chemical properties that are prepared under ultrasound irradiation causes this technique more powerful with respect to others. Ullah et. al was synthesized novel material $PtSe_2$-graphene/TiO_2 nanocomposites through a facile ultrasonic assisted method. The investigation of catalytic behavior of this nanocomposite for the decomposition of rhodamine B as a standard dye showed its enhanced photocatalytic activities due to a precise band gap in the visible range [21]. In a review article, Morsali's research group presented some applications of ultrasound irradiation, as a facile, environmentally friendly, and versatile synthetic tool for the synthesis of nanoscale metal-organic coordination polymers . This review also investigates the effects of synthetic parameters such as concentrations of initial reagents, temperature, sonication power, and solvent composition on the size and structure of the product [22]. Aggregation-induced emission (AIE)-active fluorescent organic nanoparticles (FNPs) have been extensively explored for fluorescence ''turn-on" bio-imaging applications with the unique advantages over conventional FNPs. Transformation of AIE-active molecules into FNPs can greatly expand their biomedical application potential. Zhang and co-workers reported a novel ''one-pot" strategy for fabricating AIE-active FNPs through an ultrasonic-assisted, catalysts-free and solvent-free Kabachnik-Fields (KF) reaction for the first time. The KF reaction was completed within 10 min. to generate AIE-active PTH-CHO-PEI-DEP FNPs [23].

In recent years, a great deal of research efforts is concentrated on semiconductor nanostructured materials due to their unique size and shape dependent properties. One of

them, cadmium oxide (CdO), is an n-type semiconductor with a wide direct band gap (2.77 eV) and a narrow indirect band gap (0.55 eV) [24]. This compound is applicable in some areas such as solar cells [25], transparent electrodes [26], photodiodes [27], phototransistors [28] and gas sensors [29]. Among different methods used for preparation of cadmium oxide nanoparticles, thermal decomposition of cadmium coordination compounds is noteworthy because this method has advantages such as simplicity, relatively lower temperature and solvent-free conditions.

In continuation of our program [30-34], here, the sonication-assisted synthesis and structural investigation of a new cadmium coordination compound containing a Schiff base ligand based on diethylenetriamine is reported. Furthermore a combination study including crystal structure, Hirshfeld surface analysis, TD-DFT and NBO analyses is carried out. Finally, synthesized nanostructure complex was used as precursor for the preparation of cadmium oxide nanoparticles.

2. Experimental

2.1. Materials and methods

All chemicals used in synthetic process were of reagent grad and were purchased from commercial sources and used as received. A BUCHI B-545 instrument was used for measuring of melting point. Electronic spectra were recorded on a JASCO-V570 spectrophotometer in the range of 200– 800 nm using 5×10^{-5} mol.L^{-1} of solution in dimethylsulfoxide (DMSO) solvent. The FT/IR spectra of the compounds as KBr discs were recorded by a JASCO-680 in the range of 4000–400 cm^{-1}. The instrument applied for recording of the ^{1}H and ^{13}C NMR spectra of compounds was a Bruker DPX FT/NMR-400 spectrometer. The molar conductivity of the compounds was determined by a metrohm-712 conductometer with a dip-type conductivity cell made of platinum black in 10^{-3} mol.L^{-1} of dimethylformamide(DMF) solution at 25±1°C. Thermal analyses (TG/DTG) of the complex were carried out by a Perkin-Elmer Pyris model instrument from 25 to 800 °C under nitrogen atmosphere at a heating rate of 10 °C. min^{-1}. Scanning electron microscopy (SEM) images were taken on a Hitachi S-1460 field emission scanning electron microscope using 15 kV Ac voltage. X-ray powder diffraction (XRD) measurements were performed on a STOE type STIDY-MP-Germany X-ray diffractometer with Cu Kα radiation (λ = 1.5418). The ultrasonic bath (Bandelin Super Sonorex RK-100H) with frequency of 80 kHz and 320 W was used for the sonochemical synthesis of compounds. The temperature within the reaction vessel was measured that was about 35 ºC.

2.2. Synthesis of the Schiff base ligand (L) and $CdLI_2$ complex

The preparation of the Schiff base ligand (L) and its cadmium complex was performed by sonochemical process. For the synthesis of ligand, an ethanolic mixture of N^1-(2-aminoethyl)ethane-1,2-diamine and (E)-3-(2-nitrophenyl)acrylaldehyde with 1:2 molar ratio was located in an ultrasonic bath. The progress of the reaction was monitored by TLC paper. Then, the reaction mixture of ligand was added as drop wise to an ethanolic solution of cadmium iodide salt in the ultrasonic bath. After one hour, the obtained cream precipitate was filtered and dried at 70 ˚C. Scheme 1 shows ultrasonic set up and the preparation of $CdLI_2$ nano-particles.

Color: Cream. Yield: 89%. Decomposed point: 254-256 ˚C. UV–Vis in DMSO [λ_{max}; nm (ε; $cm^{-1}M^{-1}$)]: 264(29028), 315(sh)(11566). Molar conductivity in DMF [$\Lambda°_M$; $cm^2\ \Omega^{-1}\ mol^{-1}$]: 10.84. Selected FT-IR data (KBr, cm^{-1}): 3194(m), 3054(w), 3025(w), 2915(w), 2871(w), 1639(vs), 1567(m), 1521(vs), 1427(m), 1350(vs), 1166(s), 984(s), 857(m), 788(m), 745(s), 505(w), 444(w). ^{1}H NMR (DMSO): 8.46(d, $2H_{c,c'}$, J = 8.12 Hz), 8.07(d, $2H_{i,i'}$, J = 8.00 Hz), 7.98(d, $2H_{f,f'}$, J = 7.56 Hz), 7.77(dd(t), $2H_{h,h'}$, J = 7.40 Hz, J = 7.56 Hz), 7.65(dt, $2H_{g,g'}$, J = 7.92 Hz, J = 9.24 Hz), 7.61(d, $2H_{e,e'}$, J = 16.28 Hz), 7.41(dd, $2H_{d,d'}$, J = 15.32 Hz, J = 8.92 Hz), 3.65(bs, $4H_{a,a'}$), 2.85(bs, $4H_{b,b'}$ and $1H_{NH}$) ppm.

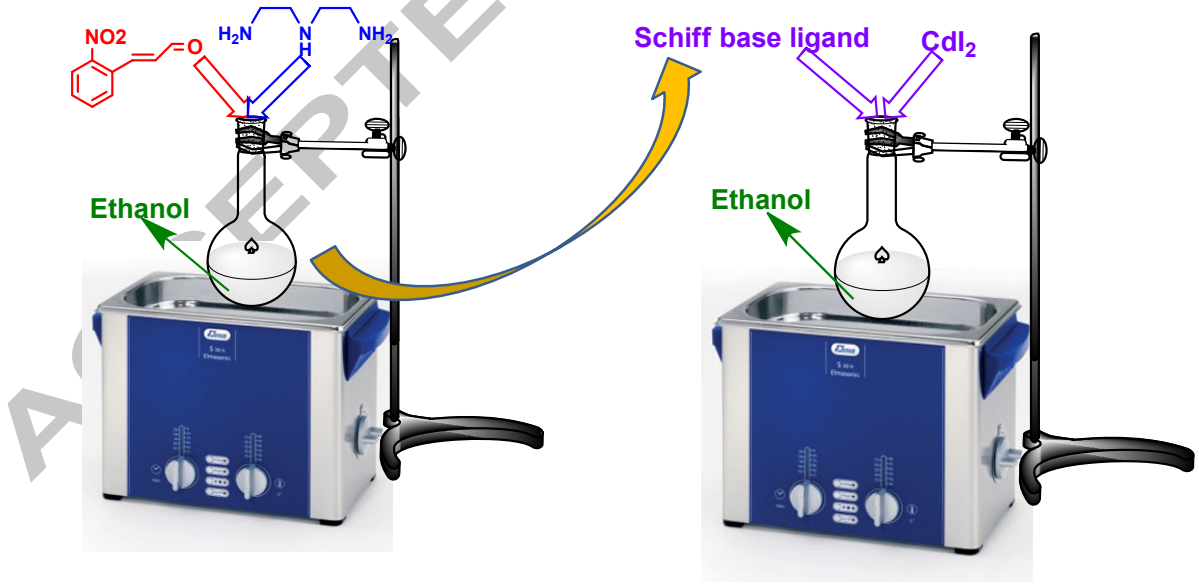

Scheme 1. Schematic ultrasonic set up for the preparation of nanostructure $CdLI_2$ complex.

2.3. Preparation of cadmium oxide nano-particles

Cadmium (II) oxide nanoparticles were prepared via direct calcination of the $CdLI_2$ complex. Accordingly appropriate amount of the nanostructured cadmium complex was transferred

into a porcelain crucible and then heated up to 600 ˚C in a furnace under air atmosphere. After about three hour, the resultant powder was washed with a little amount of acetone solvent to remove any organic impurity, and then the product was dried at 60 ^{O}C. The calcination product was analyzed using SEM and XRD methods. Scheme 2 shows synthetic route from Schiff base ligand to cadmium oxide nanoparticles.

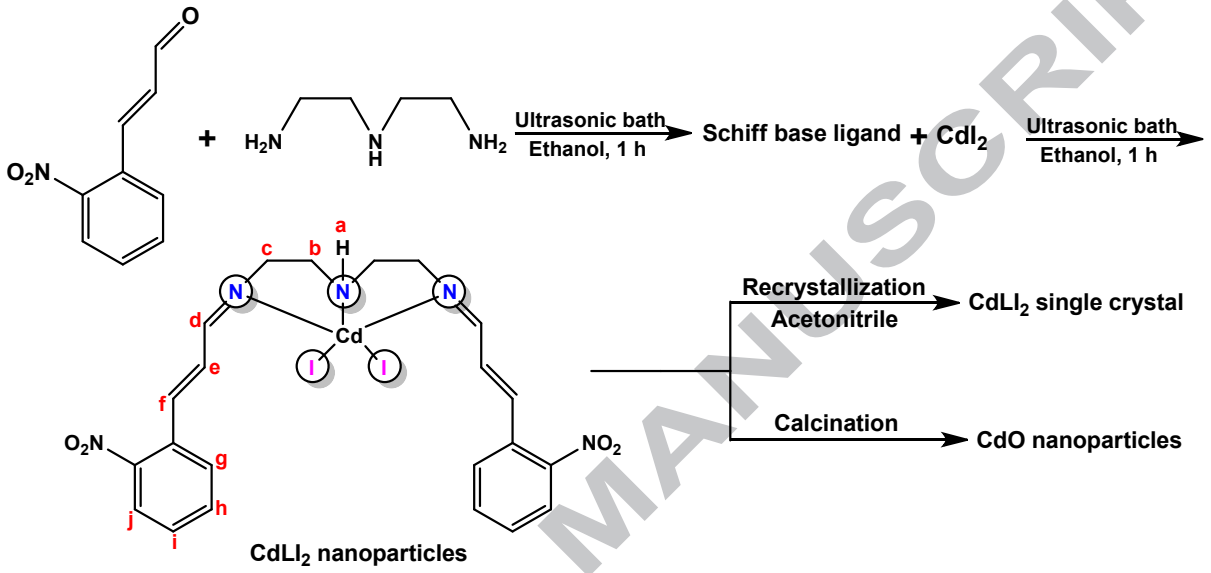

Scheme 2. Synthetic route from ligand to cadmium oxide nanoparticles.

2.4. Crystallography

Single crystal X-ray data for the cadmium iodide complex were collected at 296 K using a Bruker Kappa *Apex II* diffractometer with graphite-monochromatized Mo-Kα radiation (λ= 0.71073 Å). Data were corrected for Lorentz and polarization effects. Absorption corrections were based on fitting a function to the empirical transmission surface as sampled by multiple equivalent measurements using the SADABS part of the APEX II package since there were no clear faces for indexation. The structure was solved by direct methods and refined by full-matrix least-squares based on F^2 with SHELXTL [35]. In addition, MERCURY [36] and OLEX [37] softwares have been used for generating the molecular and packing diagrams.

2.5. Computational details

Molecular Hirshfeld surface analysis (HS) and the associated 2D fingerprint plots (FP) [38-41] were performed using Crystal Explorer [42] computer program with taking X-ray crystallography data as input. DFT calculations were carried out using Gaussian 03W program package [43]. Molecular structure was optimized using the B3LYP (Becke's three parameter hybrid functional using the LYP correlation functional) approach in conjunction

with the LANL2DZ basis set [44]. No symmetry constrains were applied during the geometry optimization. NBO calculations [45] were performed using NBO 3.1 program [46] as implemented in the GAUSSIAN 03W package at the DFT/B3LYP/LANL2DZ level in order to understand various second-order interactions between the filled orbital of one subsystem and vacant orbital of another subsystem, which is a measure of the intermolecular and intra-molecular delocalization or hyper conjugation. For calculating the excited state properties, time-dependent density functional theory (TDDFT) [47] was employed at the B3LYP/LANL2DZ level using dimethyl sulfoxide (DMSO) as solvent and the excitation energies, oscillator strengths and orbital contribution for the lowest 50 singlet-singlet transitions at the optimized geometry in the ground state were obtained.

3. Results and discussion

Cadmium iodide complex was synthesized by the sonochemical process and then, the sonication product was identified by several techniques such as XRD, SEM, FT/IR, NMR, and single crystal X-ray crystallography.

3.1. XRD and SEM

Fig. 1 shows two XRD patterns for the cadmium iodide complex. The A and B patterns are related to sonication-assisted prepared complex and its single crystal, respectively. The B pattern was simulated via MERCURY software [36]. A comparison between two XRD patterns indicates the acceptable matches with slight differences in 2θ values, confirming identical crystalline phase for two samples. The significant broadening of the peaks in the XRD pattern of sonication-assisted prepared compound states that the particles are in nanometer dimensions. The estimation of average size of particles by Scherrer's equation ($D = \frac{k\lambda}{\beta Cos\,\theta}$, where D is the average grain size, ?? is Blank's constant (0.891), λ is the X-ray wavelength (0.15405 nm), θ and β are the diffraction angle and full-width at half maximum of an observed peak, respectively) [48] gives the value about 26 nm for cadmium iodide complex. Fig. 2 illustrates the SEM image that shows morphology of cadmium complex. As observed in fig.2, the particles are agglomerated nono-spheres with an almost uniform distribution.

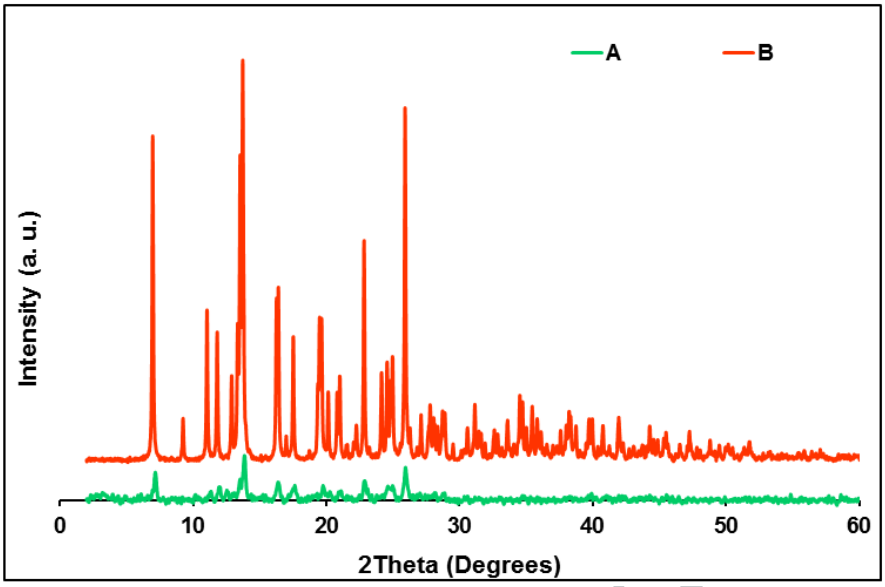

Fig. 1. The XRD patterns of cadmium iodide complex (A) prepared by sonochemical process (B) simulated from single crystal X-ray data.

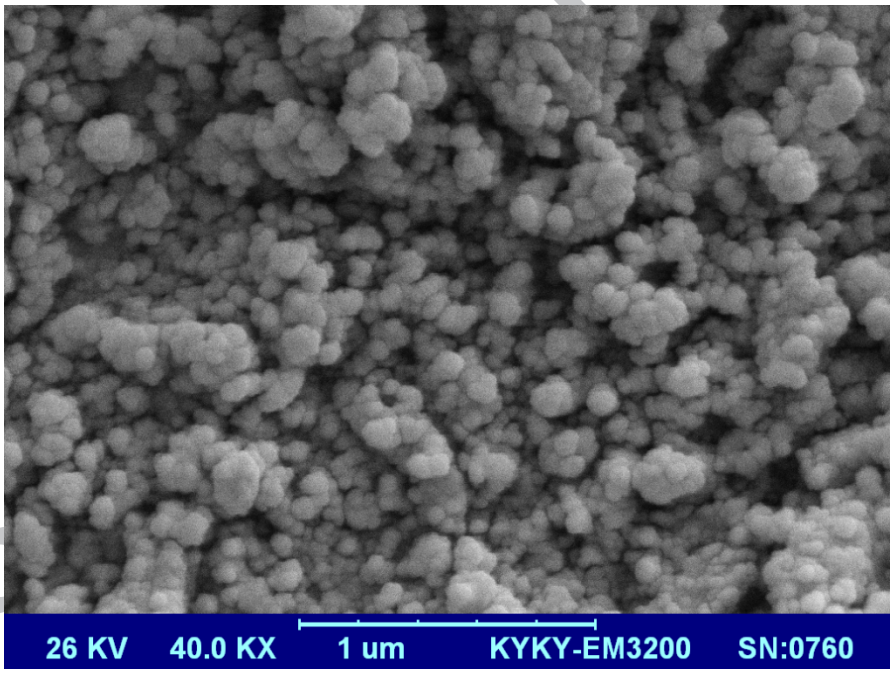

Fig. 2. SEM image of $CdLI_2$ complex prepared by sonochemical process.

3.2. FT/IR spectroscopy

The FT/IR spectra of sonochemically prepared cadmium complex and single crystal one have been exhibited in Fig. 3. Both spectra have identical patterns indicating the similar structure for both samples. Some selected vibrational frequencies and their assignments have been listed in experimental section. The characteristic peak observed at 1639 cm^{-1} is assigned to iminic bonds (C=N) that participate in coordination to metal ion [49]. The frequency related to N–H vibration of secondary amine group involved in coordination appears as a medium peak at 3200 cm^{-1}. Further evidence for coordination of the Schiff base ligand to metal center

is the appearance of a weak peak in the region of 400-500 cm^{-1} attributing to stretching vibrations of Cd-N bonds [50]. Vibrational stretching frequencies of iminic, aromatic, alkenic and aliphatic C–H bonds are found in the range of 2871 to 3065 cm^{-1}. The asymmetric and symmetric vibrations of nitro substituent of aromatic rings appear as two sharp peaks at 1521 and 1348 cm^{-1}, respectively.

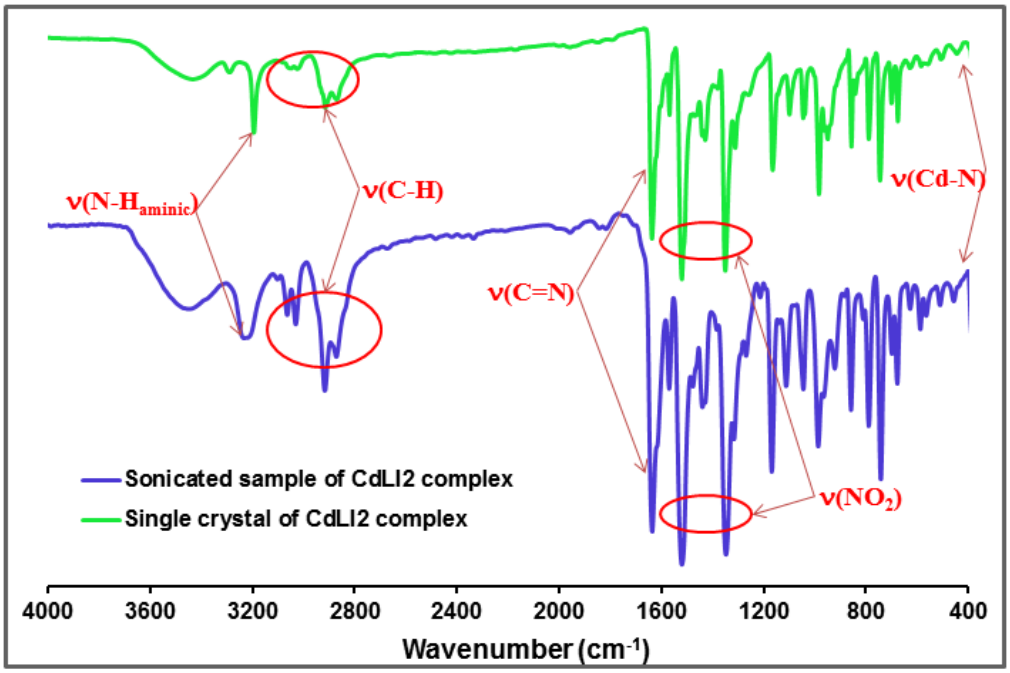

Fig. 3. The FT/IR spectra of sonochemically prepared cadmium iodide complex and its single crystal.

3.3. NMR spectroscopy

Fig. 4 shows the ^1H NMR spectrum of cadmium iodide complex in DMSO-d6-solvent. The chemical shift and coupling constant of the hydrogens are found in the experimental section regarding to the structure shown in Scheme 2. A doublet peak at 8.46 ppm is assigned to the iminic proton of H_d that is due to coupling with alkenic proton of H_e. An observed shift of this peak to downer field as compared with Schiff base ligand [49] confirms the participation of iminic nitrogens in the coordination [51,52]. There are four aromatic hydrogens in the structure of complex that appear in the range of 7.65 to 8.07 ppm. The hydrogens of H_g and H_j are observed as doublet peaks at 7.98 and 8.07, respectively. The hydrogens of H_h and H_i are observed at 7.65 and 7.77 ppm, respectively. The signal related to alkenic hydrogen of H_f appears as a doublet peak with coupling constant of 16.28 Hz at 7.39 ppm. The distinct doublet of doublet peak at 7.41 ppm is due to coupling of alkenic hydrogen of H_e with hydrogens of H_f (J = 15.32 Hz) and H_d (J = 8.92 Hz). Two other signals in the ^{1}HNMR spectrum (a sharp peak at 3.65 ppm for the H_c hydrogens and a broad singlet at 2.85 ppm for

H_a and H_b hydrogens) are assigned to the aminic part of ligand. In this way, the ^{1}HNMR spectral data well support the suggested structure.

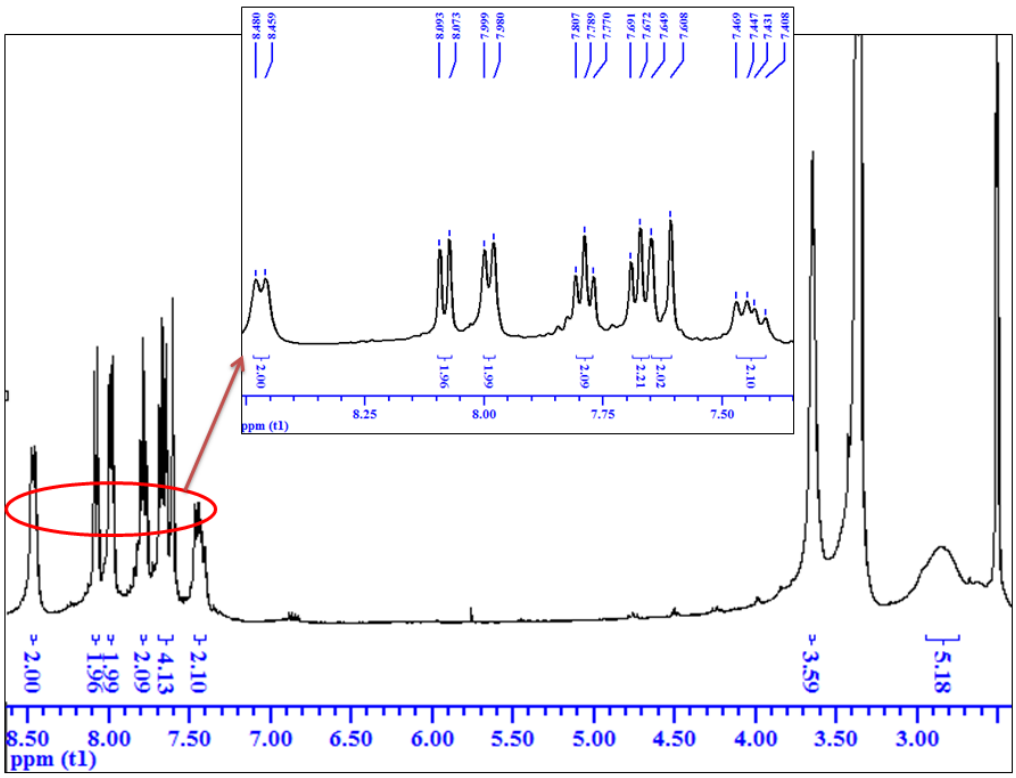

Fig. 4. ^{1}HNMR spectrum of $CdLI_2$ complex.

3.4. Crystal structure of the $CdLI_2$ complex

The crystallographic data of $CdLI_2$ complex has been summarized in Table 1. These data reveal that $CdLI_2$ complex crystallizes in Orthorhombic *Pbca* space group. The Fig. 5 shows the crystal structure of the complex and Table 2 tabulates the selected bond lengths and angles. The metal center in this mononuclear complex is five-coordinated by three nitrogen atoms from Shiff base ligand and two iodide anions (I1 and I2). Schiff base ligand (L) acts as a tridentate N_3-donor ligand and connects to metal via two iminic nitrogen (N1 and N2) and one aminic nitrogen (N3). In five-coordinated compounds, a trigonality index (τ_5) is used for the suggsetion of coordination geometry around metal center. Based on this index proposed by Addison and Reedijk, ($\tau_5 = (\beta–\alpha)/60$; where α and β are the two largest bond angles in the metal coordination sphere), the values of $\tau_5 = 0$ and 1 propose the perfect square pyramidal and trigonal bipyramidal geometries, respectively [53]. In current $CdLI_2$ complex structure with the values of α = 126.88(4)° and β = 147.02(2)°, trigonality index (τ_5) was evaluated equal to 0.33 proposing a distorted square pyramidal geometry around cadmium center. In this geometry, the square base is formed by two iminic nitrogens (N1 and N2) of Schiff base ligand and two iodide anion (I1 and I2) while the apical position is occupied by aminic

nitrogen (N3). Evaluation of bond angles around the metal center indicates all these angles deviate considerably from ideal angles of 90° or 180°, which may be attributed to the restriction induced by the two five-membered chelate rings of Cd1–N1–C11–C10–N3 and Cd1–N2–C21–C22–N3. The comparison of bite angles in zinc, cadmium and mercury iodide complexes of Schiff base ligand (L) indicates that the values of two bite angles in $CdLI_2$ complex (72.11(2)° and 74.93(2)°) are smaller than $ZnLI_2$ complex (78.40(4)° and 78.07(4)°) and larger than $HgLI_2$ complex (70.92(3)° and 71.56(3)°) [49,54]. The cadmium atom departs 0.268 Å from the mean basal plane defined by N1, N2, I1 and I2. Two basal atoms of N1 and N2 are respectively deviated 0.929 and 0.969 Å towards the apical nitrogen (N3), while two other basal atoms (I1 and I2) are deviated 0.928 and 0.980 Å to the opposite side with the apical atom, respectively. The bond length of $Cd–N_{imine}$ (2.405 and 2.414 Å) is shorter than obtained values (2.465 and 2.515 Å) for a penta-coordinated cadmium bromide complex with a tridentate Schiff based ligand based on diethylenetriamine [55] but these values are longer than reported values for Cd(II) complexes with pentadentate Schiff based ligands based on diethylenetriamine [8,56]. The $Cd–N_{amine}$ bond length (2.248 Å) is shorter than $Cd–N_{imine}$ bond lengths as seen in penta-coordinated cadmium bromide complex reported by our group previously [55] and in contrast with obtained values for cadmium complexes with pentadentate Schiff based ligands based on diethylenetriamine [8,56]. The distance of Cd–I bonds (2.722 and 2.726 Å) are close to each other and comparable with their values in cadmium(II) complexes with a CdI_2N_3 coordination environment (2.722 and 2.726 Å in $C_{23}H_{23}Cd_1I_2N_3S_2$ [57] and 2.724 and 2.742 Å in $C_{37}H_{28}Cd_1I_2N_4S_1$ [58].

The crystal packing analysis shows the intermolecular interactions such as C–H···O, C–H···I and π···π interactions in the structure of $CdLI_2$ complex that organize the self-assembly process. These interactions are related to phenyl rings and their nitro substituent and also coordinated iodide anions. From Table 3, the O2 and O4 atoms (hydrogen bonding acceptors) of two nitro substituents form C–H···O interactions with the aliphatic hydrogens of H10B and H10A, respectively. Each molecule participates in the formation of four C–H···O hydrogen bonds for connecting to two adjacent molecules via macrocyclic graph sets of $R_2^2(24)$. Fig. 6 shows the extension of C–H···O interactions as a one-dimensional supramolecular chain. Also, the weak C–H···I hydrogen bonds are formed via the interaction of coordinated iodide anions (as acceptor) with alkenic carbons of C3 and C14 as donor (Table 3). Each molecule interacts with four adjacent molecule by the one of participating atoms in the formation of two types of C–H···I hydrogen bond, resulting to 2D

supramolecular structure (Fig. 8). In addition to, the phenyl rings are involved in the formation two types of π-π stacking interactions. The geometrical parameters related to these interactions have been listed in Table 4 which is close to the accepted values for the strong π-interactions [59]. Each ring is stacked over two aromatic rings of two neighbor molecule and each molecule is in contact with three neighbor molecule (from one side with one molecule and other side with two molecules) by four π-π interactions (Fig. 8).

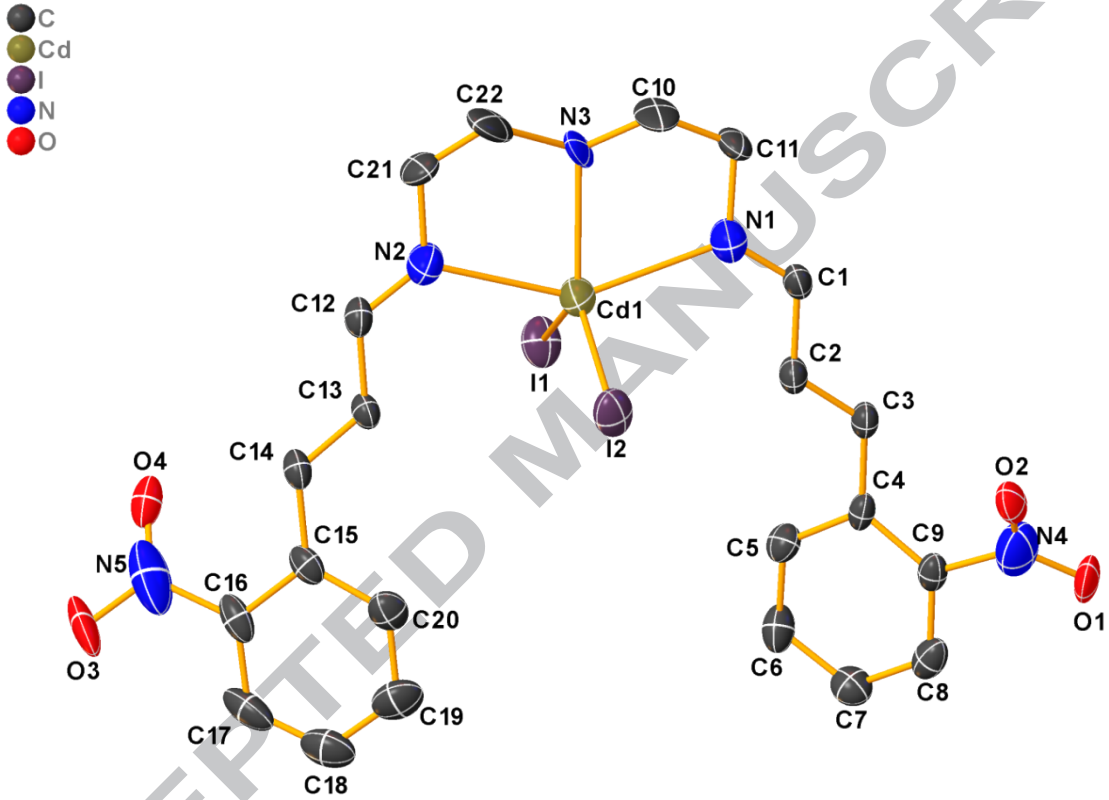

Fig. 5. The crystal structure of $CdLI_2$ complex with atomic numbering scheme. Hydrogen atoms are omitted for more clarity.

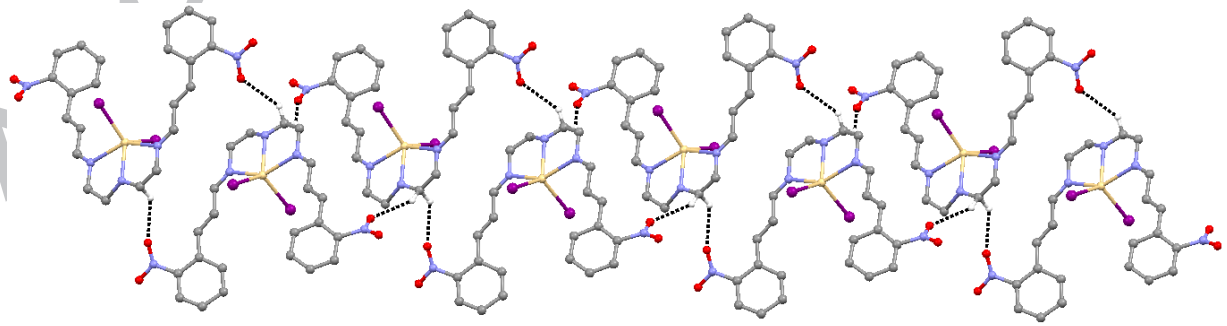

Fig. 6. One-dimensional supramolecular chain of C–H···O interactions in the structure of $CdLI_2$ complex.

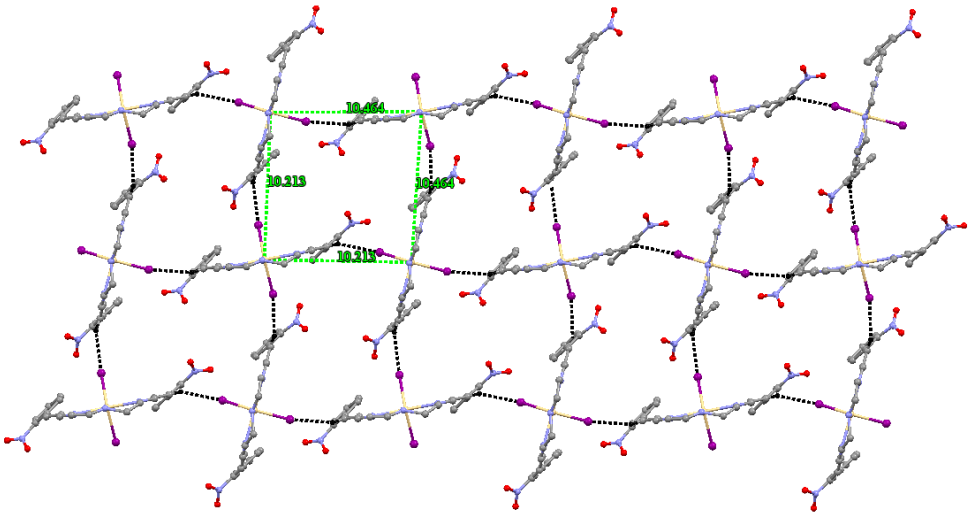

Fig. 7. 2D extension of C–H···I interactions in the structure of $CdLI_2$ complex.

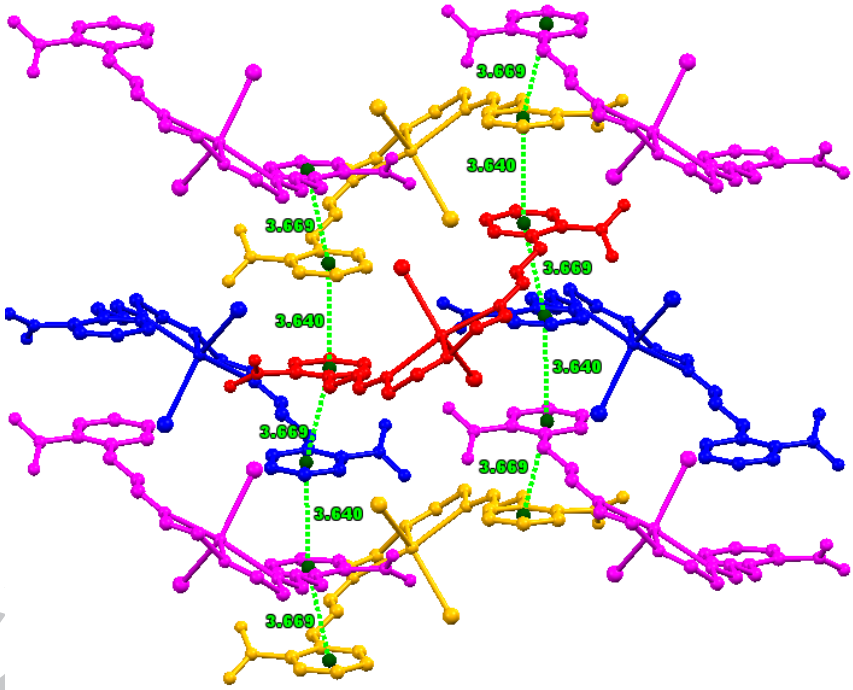

Fig. 8. π-π interactions in the structure of $CdLI_2$ complex.

Table 1
Crystal data and structure refinement for $CdLI_2$ complex.

Compound	$CdLI_2$
Chemical formula	$C_{22}H_{23}N_5O_4CdI_2$
Formula weight	787.65
Crystal system	Orthorhombic
Crystal size (mm)	0.13 × 0.12 × 0.04
space group	*Pbca*
Temperature (K)	296
Wavelength (Å)	0.71073
a (Å)	14.9787 (3)
b (Å)	14.2518 (2)
c (Å)	25.3466 (5)
V (Å^3)	5410.83 (17)

Z	8
D_{calc} (Mg/m^3)	1.934
μ (mm^{-1})	3.13
F(000)	3008
Absorption correction	Multi-scan *SADABS*
Theta range for data collection (°)	1.5 to 30
Index ranges	*-19 ≤ h ≤ 19*
	-18 ≤ k ≤ 18
	-33 ≤ l ≤ 0
Maximum and minimum transmission	0.746, 0.659
Refinement method	Full-matrix least-squares on F^2
Reflections collected	24780
independent reflections	6523
R_{int}	0.065
Goodness-of-fit (GOF) on F^2	1.34
$R[F^2 > 2s(F^2)]$	0.084
$wR(F^2)$	0.141
Data/restraints/parameters	6523/0/308
Largest difference in peak and hole (e $Å^{-3}$)	2.07 and -0.76

Table 2

Selected experimental and calculated bond lengths (Å) and angles (°) at B3LYP/LANL2DZ level of cadmium iodide complex.

Parameter	Experimental	Calculated	Deviation (%)
Bond length (Å)			
Cd–N1	2.405(7)	2.478	3.03
Cd–N2	2.414(7)	2.462	1.99
Cd–N3	2.248(7)	2.455	9.21
Cd–I1	2.722(10)	2.856	4.93
Cd–I2	2.723(10)	2.874	5.44
Bond angle (°)			
N1–Cd–N2	147.1(2)	143.90	2.17
N1–Cd–N3	72.1(2)	71.37	1.01
N1–Cd–I1	97.91(18)	100.44	2.58
N1–Cd–I2	98.11(18)	95.42	2.74
N2–Cd–N3	75.0(2)	72.54	3.28
N2–Cd–I1	98.29(18)	99.10	0.82
N2–Cd–I2	94.77(19)	96.72	2.06
N3–Cd–I1	118.16(18)	121.52	2.84
N3–Cd–I2	114.96(18)	111.65	2.88
I1–Cd–I2	126.88(4)	126.83	0.04

Table 3

Intermolecular interactions in structure of $CdLI_2$ complex.

Interaction	D–H···A	D–H (Å)	H···A (Å)	D···A (Å)	A···H–D (°)	Symmetry code
C–H···O	C10–H10B···O2	0.970	2.520	3.33(2)	141	-1/2+x,y,1/2-z
	C10–H10A···O4	0.970	2.475	3.23(2)	134	-1/2+x,y,1/2-z
C–H···I	C14–H14A···I1	0.930	3.009	3.856(9)	152	1/2-x,-1/2+y,z
	C3–H3A···I2	0.929	3.052	3.926(8)	157	-1/2-x,1/2+y,z

Table 4

π-π interactions in structure of $CdLI_2$ complex.

Compound	π–π interactions	$d_{π–π}$ (Å)	Dihedral angle (˚)	Shift distance (Å)	symmetry code
$CdLI_2$	Cg(1)···Cg(2)	3.640	5.949	0.325	-x,1-y, -z
	Cg(1)···Cg(2)	3.669	5.781	1.130	-1/2+x,1/2-y,-z

Ring code: Cg(1):C4, C5, C6, C7, C8, C9; Cg(2):C15, C16, C17, C18, C19, C20.

3.5. Hirshfeld surface analysis

Hirshfeld surface analysis was carried out based on the single crystal X-ray data for the investigation the nature and quantitative contributions of intermolecular interactions in the crystal packing of $CdLI_2$ complex. The Hirshfeld surfaces mapped on the d_{norm} (ranging from -0.15 (red) to 1.46 (blue) Å) and shape index (1.0 (concave) to 0.1 (convex) Å) have been shown in Fig. 9, respectively. The surfaces are exhibited as transparent to allow visualization of the molecular moiety around the calculated part. The red spots appeared on the d_{norm} surface of the complex are in agreement with intermolecular interactions listed in Table 3 and the white regions are attributed to the weaker and longer contacts. The surface mapped on d_{norm} function shows eight red spots on the front and back sides of the molecule related to non-classical hydrogen bonds of C–H···O and C–H···I interactions. O... H/H... O contacts appear as four red pots around the O2 and O4 atoms as acceptor and H10A and H10B of C10 atoms as donor. Four other red pots observed on d_{norm} surface are due to I... H/H... I interactions. Evaluation of Hirshfeld surfaces of cadmium complex under the *shape index* function shows red–blue triangle regions (bow–tie patterns) which are attributed to π-π stacking interactions.

2D Fingerprint plots corresponded to Hirshfeld surfaces are represented as plots of d_i versus d_e. These plots can be divided to quantify the contributions of intermolecular interactions [40]. Fig. 10 shows 2D fingerprint plots of Hirshfeld surface for the $CdLI_2$ complex. Complementary regions are visible in the fingerprint plots where one molecule act as donor ($d_e > d_i$) and the other as an acceptor ($d_e < d_i$). The H... H close contacts have the highest contribution of the total Hirshfeld surface with a share of 30.8%. This high share is an obvious result for the compounds with a high percentage of hydrogen atoms in the structure [60], even though does not lead to a directional role for H...H contacts. The second share of entire surface is related to O... H/H... O contacts (24.6%) that are observed as two distinct spikes in the middle part of plot. I... H/H... I contacts forms 18.7% of total surface and are obvious as two partly sharp spikes with the shortest close-contact distance ($d_i + d_e \approx 2.86$ Å) in the outer parts of plot. C... H/H... C contacts (mainly representing C–H... π interactions) comprise 12% of entire surface that are observed as two partly wide wing-like spikes. C...C close contacts (attributed to π... π interactions) form 7.3% of all contacts. The remaining Hirshfeld surface is due to non-directional interactions such as N...H/H...N, O...I/I...O, I...N/N ...I and O...N/N...O with the share of 2.1, 1.1, 0.9 and 0.8%, respectively.

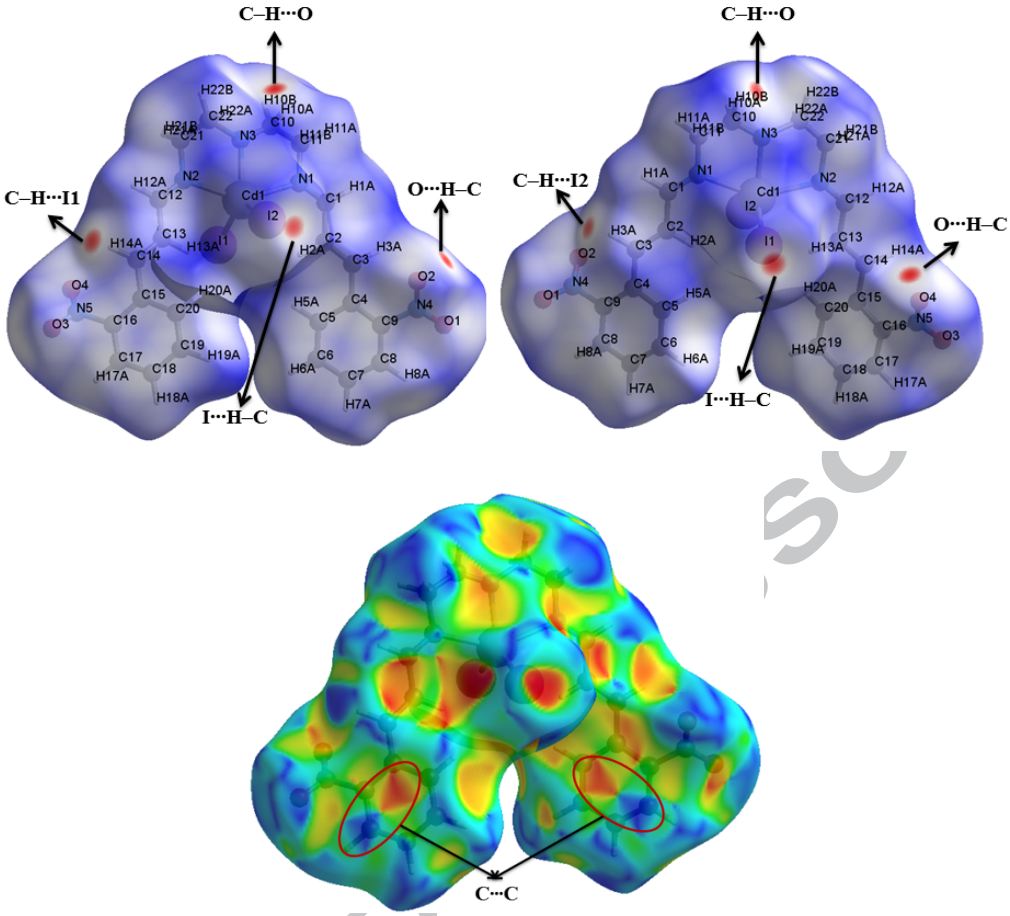

Fig. 9. The Hirshfeld surfaces of $CdLI_2$ complex mapped over d_{norm} (up) and *shape index* (down).

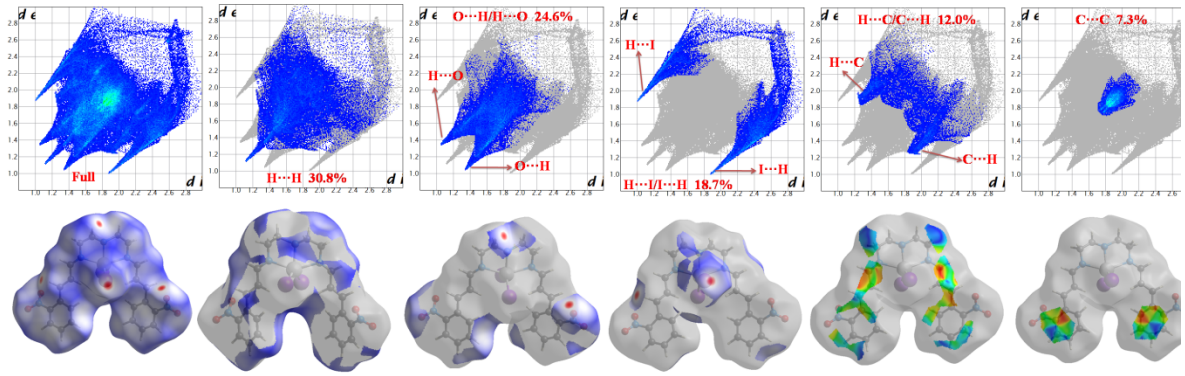

Fig. 10. 2D fingerprint plots (up) and Hirshfeld surfaces (down) of the different interactions in the structure of $CdLI_2$ complex.

3.6. Thermal analysis

For the investigation of thermal behavior of the cadmium iodide complex, thermogravimetric analysis (TG/DTG) was carried out in the temperature range of 25 to 800 °C with the heating rates of 10 °C. min^{-1} under a static nitrogen atmosphere. TG curve of $CdLI_2$ complex (Fig. 11) suggests thermal decomposition of the compound in two steps. The first thermal decomposition step is occurred in the temperature range of 218 to 295 °C accompanied by a

mass reduction about 30% (calculated 31%) that was attributed to loss of two aromatic rings bearing nitro groups. The peak temperature (T_{max}) of this step is 236.7 °C. The second thermal decomposition step happens at 295-685 °C with a mass loss about 54.7% (calculated 54.9%) of the total molecular weight assigned to elimination of residual parts of Schiff base ligand and two coordinated iodide anions. The final residual fragment with the mass about 15.7% (calculated 14.2%) corresponds to cadmium metal.

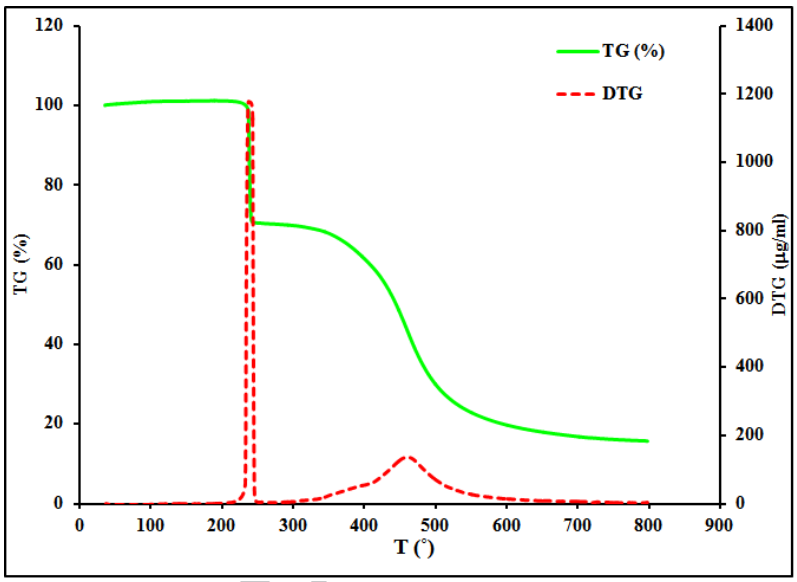

Fig. 11. TG/DTG curves of $CdLI_2$ complex.

3.7. DFT calculations

3.7.1. Geometry optimization

Fig. 12 shows the superimposition of crystallographic structure of $CdLI_2$ complex (red color) and the optimized molecular structure obtained at the B3LYP/LANL2DZ level of theory (blue color). This overlay represents nearly equal geometries with slight structural discrepancies. The calculation of the root mean square deviation (RMSD) between the x-ray crystallographic and the optimized structures can be used for finding the differences of two structures. Accordingly, the calculated value for RMSD (0.5661 Å) indicates a negligible deviation of the optimized structure from the x-ray structure. As observed in Fig. 12, in two structures, phenyl rings have a dihedral angle (5.95° in x-ray structure and 30.72° in optimized structure). Table 2 compares the experimental and theoretical values of bond lengths and angles around metal center. Based on these values, the bond lengths of theoretical structure are slightly larger than the experimental ones, while for the bond angles specified trend was not observed. The most deviation of bond lengths is related to $Cd–N_{aminic}$ (0.207 Å (9.21%)). The theoretical bond angles indicate low deviation up to 3.28% for the chelate angle of N2–Cd–N3 with respect to x-ray structure. The observed differences may be

attributed to the calculation method, and the effects of crystal packing in solid state [61]. On the basis of DFT calculations, the value of trigonality index (τ_5) is 0.28 which suggests a distorted square pyramidal geometry around cadmium center, matching with suggested geometry using the X-ray crystallographic data.

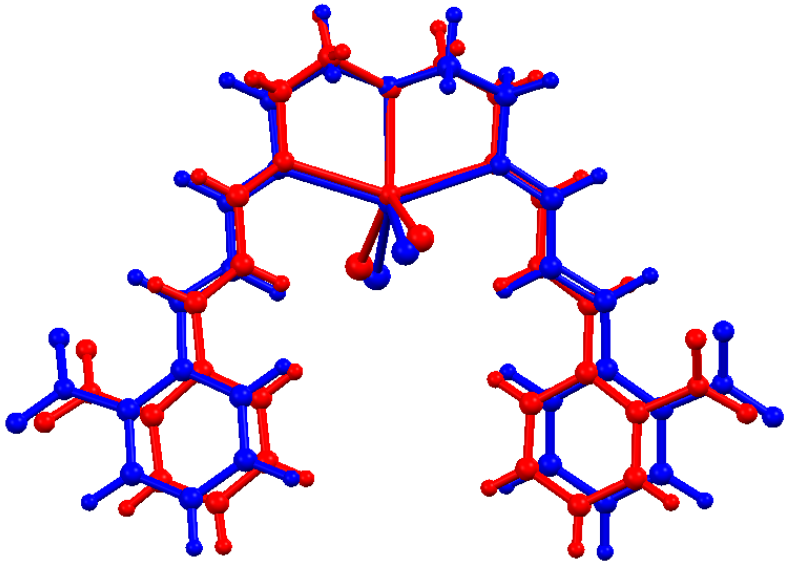

Fig. 12. Atom-by-atom superimposition of $CdLI_2$ complex (red: calculated and blue: X-ray structure)

3.7.2. UV-visible spectrum and TD-DFT calculations

Fig. 13 shows the experimental and theoretical UV-Vis spectra of cadmium iodide complex in DMSO solvent. In the range of 200-800 nm, the complex indicates two absorption bands. The first absorption band as a strong peak at 264 nm (ε= 29028 $M^{-1}.cm^{-1}$) is assigned to intra-ligand $\pi \rightarrow \pi^*$ electronic transitions of the phenyl rings, olefinic and azomethine bonds of coordinated Schiff base ligand [62]. The second absorption band as a shoulder peak at 315 nm (ε= 11566 $M^{-1}.cm^{-1}$) is due to $d \rightarrow \pi^*$ transitions. In the visible region of the spectrum, no band related to d-d transitions is observed that is in accordance with the d^{10} configuration of the Cd(II) ion [63].

For more concise investigation of the electronic transitions in cadmium iodide complex, TD-DFT calculation was carried out at the B3LYP/LANL2DZ method in DMSO solvent. Table 5 summarizes the strong transitions with an oscillator strength > 0.12 and their major contribution and character. The most important transition is the forty-eighth excited state at 274.56 nm with an oscillator strength of 0.5258. This transition is due to the promotion of electron from HOMO-12 → LUMO (19%), HOMO-12 → LUMO+1 (11%) and HOMO-14 → LUMO+1 (10%). The HOMO-12 and HOMO-14 is mostly localized on one of the oxygen

atoms of nitro groups, while LUMO and LUMO+1 is delocalized on the π* orbitals of nitro groups. Therefore, these transitions are attributed to an intraligand charge transfer (ILCT). Other important transition is the forty second excited state at 290.51 nm with an oscillator strength of 0.3592 that corresponds to the raise of electron from HOMO-6 → LUMO+3 (37%). HOMO-6 and LUMO+3 are mostly delocalized on π(C) orbitals of aromatic ring and π* orbitals of iminic bonds, respectively. So, this transition is an intraligand charge transfer (ILCT). Also, another important transition is observed at 284.51 nm with an oscillator strength of 0.2093 relating to the promotion of electron from HOMO-4 → LUMO+2 (31%). HOMO-4 is spread on π(C) orbitals of one of the aromatic rings. The acceptor orbital of LUMO+2 is mostly delocalized on cadmium atom (55%) and two coordinated iodide anions (24%). Accordingly, this transition is attributed to the combination of metal-to-ligand charge transfer (MLCT) and ligand-to-ligand charge transfer (LLCT). Furthermore, two another transitions are observable at 445.74 and 442.08 nm with oscillator strengths of 0.1313 and 0.1260, respectively. The major contribution of these two transitions is due to the transition of electron from HOMO-4 → LUMO (59%) and HOMO-4 → LUMO+1 (46%), respectively. According to the contribution of molecular orbitals, these electronic transitions are intraligand charge transfer (ILCT) type.

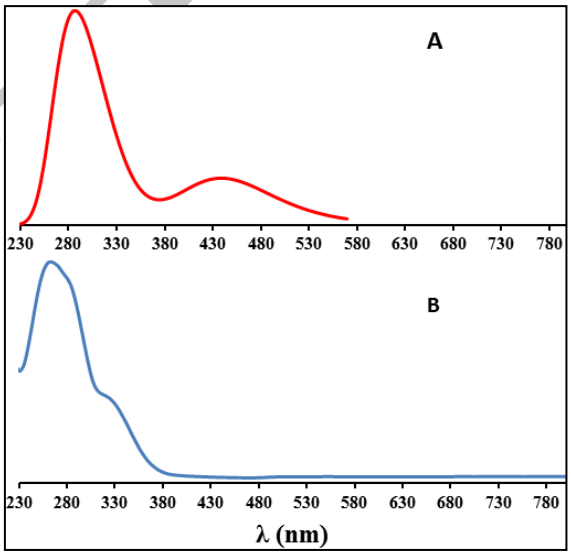

Fig. 13. The theoretical (A) and experimental (B) UV-vis spectra of $CdLI_2$ complex in DMSO solvent.

Table 5
Wavenumber (in nm), oscillator strength (f_{osc}), main orbital contributions, and type of transition involved in the most important excitations for $CdLI_2$ complex in DMSO solvent calculated at TDDFT/B3LYP/LANL2DZ level.

Excited State	$\lambda_{Cald.}$	Oscillator strengths (f)	Major contribution	Character

9	445.74	0.1313	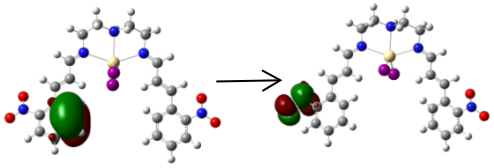 HOMO-4 LUMO	(59 %)	ILCT
10	442.08	0.1260	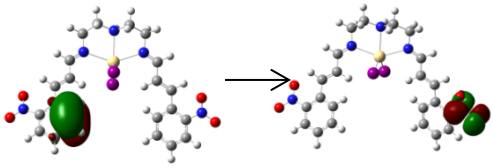 HOMO-4 LUMO+1	(46 %)	ILCT
33	315.54	0.2093	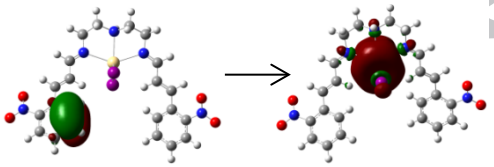 HOMO-4 LUMO+2	(31%)	LMCT/LLCT
42	290.51	0.3592	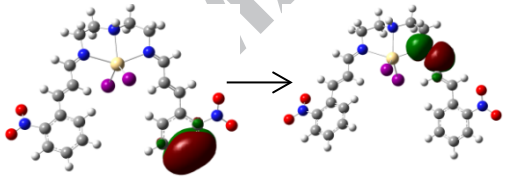 HOMO-6 LUMO+3	(37%)	ILCT
48	274.56	0.5258	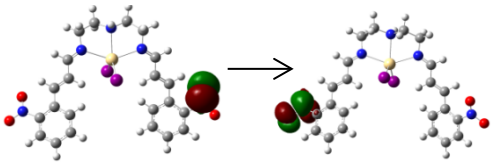 HOMO-12 LUMO	(19%)	ILCT

3.7.3. Natural bond orbital (NBO) analysis

The natural bond orbital (NBO) analysis is a powerful technique for investigation of intra- and inter-molecular bonding, interaction between bonds and also provides convenient basis to study of charge transfer or conjugative interaction in molecular systems [64]. NBO analysis of cadmium iodide complex was performed at B3LYP/LanL2DZ level of theory. Table 6 tabulates the selected donor and acceptor orbitals along with their description, hybridization of atoms, occupancy of the orbitals and the second-order stabilization energies ($E^{(2)}$). The table data was listed on the basis of optimized structure of the CdLI2 complex (Fig. 14).

The NBO analysis shows an intra-molecular hyperconjugative interaction in throughout molecule. This hyper conjugation extended in two sides of Schiff base ligand from nitro substituent of aromatic ring to imine group is a distinctive and strong interaction. The most stabilization energy for this complex is due to $\pi^* \rightarrow \pi^*$ interactions inside the aromatic rings. The charge transfer from π*(C20-C29) to π*(C25-C27) into one ring and π*(C42-C43) to π*(C44-C46) into another ring leads to stabilization energies of 233.32 and 238.11 kcal.mol^{-1}, respectively. The donor anti-bonding orbitals of π*(C20-C29) and π*(C42-C43) participate in another charge transfer to π*(C21-C23) and π*(C48-C50), respectively, leading to stabilization energies of 168.42 and 172.18 kcal.mol^{-1}. Also, the anti-bonding orbitals of π*(C20-C29) and π*(C42-C43) as donor NBO interact with the anti-bonding orbitals of π*(C16-C18) and π*(C38-C40) outside the aromatic ring and give the energies of 53.45 and 50.10 kcal.mol^{-1} to system, respectively. The partly high electron density of π*(C20-C29) (ED = 0.44200 e) and π*(C42-C43) (ED = 0.44086 e) as anti-bonding NBOs is due to the charge transfer from bonding NBOs of π(C21-C23) (ED = 1.63112 e), π(C25-C27) (ED = 1.64132 e), σ(C18-H19) (ED = 1.97060 e), π(C16-C18) (ED = 1.80273 e) and π(N8-O10) (ED = 1.98192 e) to π*(C20-C29) and from bonding NBOs of π(C38-C40) (ED = 1.80600 e), π(C44-C46) (ED = 1.64140 e), σ(C40-H41) (ED = 1.97012 e), π(C48-C50) (ED = 1.63009 e) and π(N9-O12) (ED = 1.98219 e) to π*(C42-C43). Moreover, there is an $n \rightarrow \pi^*$ interaction with partly high stabilization energy between the atoms of nitro groups. The charge transfer of LP(3)O11 and LP(3)O13 with $sp^{99.99}$ hybridization to anti-bonding orbitals of π*(N8-O10) and π*(N9-O12) leads to the stabilization energies of 159.43 and 158.90 kcal.mol^{-1}. Also, there are several $\pi \rightarrow \pi^*$ donation with the energies in the range of 20.37- 37.42 kcal.mol^{-1}, indicating the expansion of hyper conjugation on the whole system.

The strength of interaction between metal center and coordinated atoms can be investigated by second-order perturbation energy. In this complex, the I→ Cd coordination bonds are formed by $n \rightarrow n^*$ donation from the $sp^{2.42}$ hybrid orbital of the I2 atom and the $sp^{2.40}$ hybrid orbital of the I3 atom to the $sp^{0.03}$ hybrid orbital of Cd (LP*(6)Cd1) with the donor-acceptor interaction energies of 56.11 kcal.mol^{-1} for I2 → Cd and 56.27 kcal.mol^{-1} for I3 → Cd. Also, there is a weaker I → Cd electron donation from the $sp^{2.42}$ hybrid orbital of the I2 atom and the $sp^{2.40}$ hybrid orbital of the I3 atom to the unoccupied hybrid orbital of the cadmium atom (LP*(7)Cd) with p character. The stabilization energy for all three N→ Cd coordination bonds is lower than I→ Cd bonds. For N_{imine}→ Cd coordination bonds, the highest interaction energy is due to $n \rightarrow n^*$ donation from the $sp^{2.26}$ hybrid orbital of N4 atom to $sp^{99.99}$ hybrid

orbital on the cadmium atom (LP*(8)Cd1) with the energy of 18.30 kcal.mol^{-1} and from the $sp^{2.32}$ hybrid orbital of N5 atom to $sp^{0.03}$ hybrid orbital on the cadmium atom (LP*(6)Cd1) with the energy of 15.16 kcal.mol^{-1}. $N_{amine} \rightarrow Cd$ bond has the lower stabilization energy than two $N_{imine} \rightarrow Cd$ bonds. The highest energy for this bond ($E^{(2)}$ = 9.38 kcal.mol^{-1}) is related to overlap of the $sp^{5.66}$ hybrid orbital of N6 atom with $sp^{50.31}d^{0.04}$ hybrid orbital of the cadmium atom (LP*(9)Cd1).

Table 6
Selected NBO orbitals of $CdLI_2$ complex, their description and occupancy (e), and the second-order interaction energies ($E^{(2)}$, kcal.mol^{-1}) between the donor and acceptor orbitals, calculated at the B3LYP/LANL2DZ level.

Donor NBO	ED (e)	Description of the donor orbital	Acceptor NBO	Description of the acceptor orbital	ED (e)	$E^{(2)}$ (kcal/mol)
LP(4)I2	1.71913	$sp^{2.42}$ (29.28% s, 70.72% p)	LP*(6)Cd1	$sp^{0.03}$(97.24% s, 2.62% p)	0.51574	56.11
LP(4)I2	1.71913	$sp^{2.42}$ (29.28% s, 70.72% p)	LP*(7)Cd1	p(0.01% s, 99.81% p)	0.20774	40.13
LP(4)I3	1.72318	$sp^{2.40}$ (29.41% s, 70.59% p)	LP*(6)Cd1	$sp^{0.03}$(97.24% s, 2.62% p)	0.51574	56.27
LP(4)I3	1.72318	$sp^{2.40}$ (29.41% s, 70.59% p)	LP*(7)Cd1	p(0.01% s, 99.81% p)	0.20774	37.42
π(C16-C18)	1.80273	0.72(p)C16 + 0.69(p)C18	π*(N4-C14)	0.62(p)N4 - 0.79(p)C14	0.16515	25.60
π(C20-C29)	1.61372	0.68(p)C20 + 0.73(p)C29	π*(N8-O10)	0.77(p)N8 - 0.64(p)O10	0.65804	34.52
π(C20-C29)	1.61372	0.68(p)C20 + 0.73(p)C29	π*(C25-C27)	0.70(p)C25 - 0.71(p)C27	0.28760	20.83
π(C21-C23)	1.63112	0.71(p)C21 + 0.70(p)C23	π*(C20-C29)	0.73(p)C20 - 0.68(p)C29	0.44200	23.50
π(C25-C27)	1.64132	0.71(p)C25 + 0.70(p)C27	π*(C20-C29)	0.73(p)C20 - 0.68(p)C29	0.44200	20.87
π(C25-C27)	1.64132	0.71(p)C25 + 0.70(p)C27	π*(C21-C23)	0.70(p)C21 - 0.71(p)C23	0.27408	20.37
π(C38-C40)	1.80600	0.72(p)C38 + 0.69(p)C48	π*(N5-C36)	0.62(p)N5 - 0.79(p)C36	0.16475	25.48
π(C42-C43)	1.61396	0.68(p)C42 + 0.73(p)C43	π*(N9-O12)	0.77(p)N9 - 0.64(p)O12	0.65875	34.92
π(C42-C43)	1.61396	0.68(p)C42 + 0.73(p)C43	π*(C44-C46)	0.71(p)C44- 0.70(p)C46	0.28768	20.87
π(C44-C46)	1.64140	0.70(p)C44 + 0.71(p)C46	π*(C42-C43)	0.73(p)C42- 0.68(p)C43	0.44086	20.84
π(C44-C46)	1.64140	0.70(p)C44 + 0.71(p)C46	π*(C48-C50)	0.71(p)C48- 0.70(p)C50	0.27584	20.46
π(C48-C50)	1.63009	0.70(p)C48 + 0.71(p)C50	π*(C42-C43)	0.73(p)C42- 0.68(p)C43	0.44086	23.61
LP(3)O11	1.43691	$sp^{99.99}$(0.53% s, 99.47% p)	π*(N8-O10)	0.77(p)N8 - 0.64(p)O10	0.65804	159.43
LP(3)O13	1.43847	$sp^{99.99}$(0.46% s, 99.54% p)	π*(N9-O12)	0.77(p)N9 - 0.64(p)O12	0.65875	158.90
π*(C20-C29)	0.44200	0.73(p)C20 - 0.68(p)C29	π*(C16-C18)	0.69(p)C16 - 0.72(p)C18	0.11031	53.45
π*(C20-C29)	0.44200	0.73(p)C20 - 0.68(p)C29	π*(C21-C23)	0.70(p)C21- 0.71(p)C23	0.27408	168.42
π*(C20-C29)	0.44200	0.73(p)C20 - 0.68(p)C29	π*(C25-C27)	0.70(p)C25 - 0.71(p)C27	0.28760	233.32
π*(C42-C43)	0.44086	0.73(p)C42- 0.68(p)C43	π*(C38-C40)	0.69(p)C38- 0.72(p)C40	0.10885	50.10
π*(C42-C43)	0.44086	0.73(p)C42- 0.68(p)C43	π*(C44-C46)	0.71(p)C44- 0.70(p)C46	0.28768	238.11
π*(C42-C43)	0.44086	0.73(p)C42- 0.68(p)C43	π*(C48-C50)	0.71(p)C48- 0.70(p)C50	0.27584	172.18
LP(1)N4	1.86358	$sp^{2.26}$ (30.71% s, 69.29% p)	LP*(6)Cd1	$sp^{0.03}$(97.24% s, 2.62% p)	0.51574	14.86
LP(1)N4	1.86358	$sp^{2.26}$ (30.71% s, 69.29% p)	LP*(8)Cd1	$sp^{99.99}$(0.4% s, 99.56% p)	0.16619	18.30
LP(1)N5	1.86276	$sp^{2.32}$ (30.15% s, 69.85% p)	LP*(6)Cd1	$sp^{0.03}$(97.24% s, 2.62% p)	0.51574	15.16
LP(1)N5	1.86276	$sp^{2.32}$ (30.15% s, 69.85% p)	LP*(8)Cd1	$sp^{99.99}$(0.4% s, 99.56% p)	0.16619	7.65
LP(1)N5	1.86276	$sp^{2.32}$ (30.15% s, 69.85% p)	LP*(9)Cd1	$sp^{50.31}d^{0.04}$(1.95% s, 97.97% p,0.08%d)	0.16431	10.48
LP(1)N6	1.89190	$sp^{5.66}$(15.02% s, 84.98% p)	LP*(6)Cd1	$sp^{0.03}$(97.24% s, 2.62% p)	0.51574	8.92
LP(1)N6	1.89190	$sp^{5.66}$(15.02% s, 84.98% p)	LP*(9)Cd1	$sp^{50.31}d^{0.04}$(1.95% s, 97.97% p,0.08%d)	0.16431	9.38

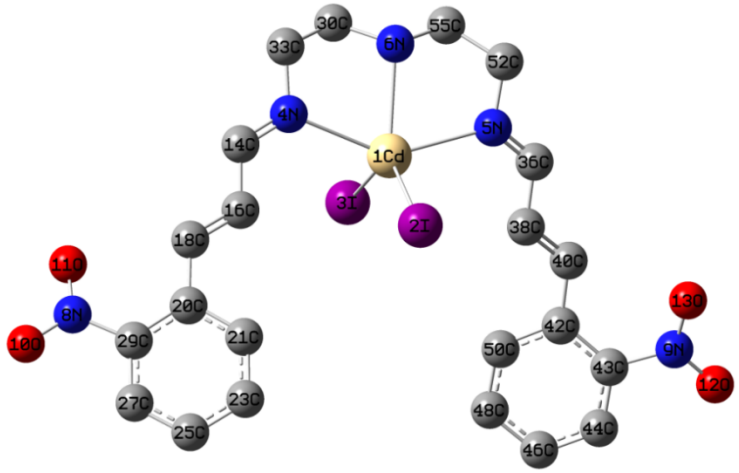

Fig. 14. Optimized structure of $CdLI_2$ complex.

3.8. Characterization of cadmium oxide nanoparticles

The characterization of the final product of direct calcination of $CdLI_2$ complex was carried out by X-ray powder diffraction (XRD). Fig. 15 illustrates the X-ray diffraction pattern of the compound obtained from thermolysis of cadmium iodide complex. In this pattern, Bragg's reflections located at about 2θ values of 32.95, 38.26, 55.24, 65.89, 69.25, 81.73, 91.01, and 94.27˚ are attributed to the crystal planes of ((111), (200), (220), (311), (222), (400), (331) and (420)), respectively. These planes are in agreement with face centered cubic (fcc) structure of CdO with standard JCPDS no. 05-0640, space group Fm3m, lattice constants; a = 0.4695 nm and Z = 4. In this XRD pattern, no other peaks related to any impurity were observed. Average crystallite size of cadmium oxide nanoparticles was evaluated by Scherrer equation and based on the highest diffraction peak (assigned to 111 crystal plane), The value was calculated to be 25 nm. Furthermore, TEM image (Fig. 15) shows that the cadmium oxide particles are nano-size, spherical and agglomerated.

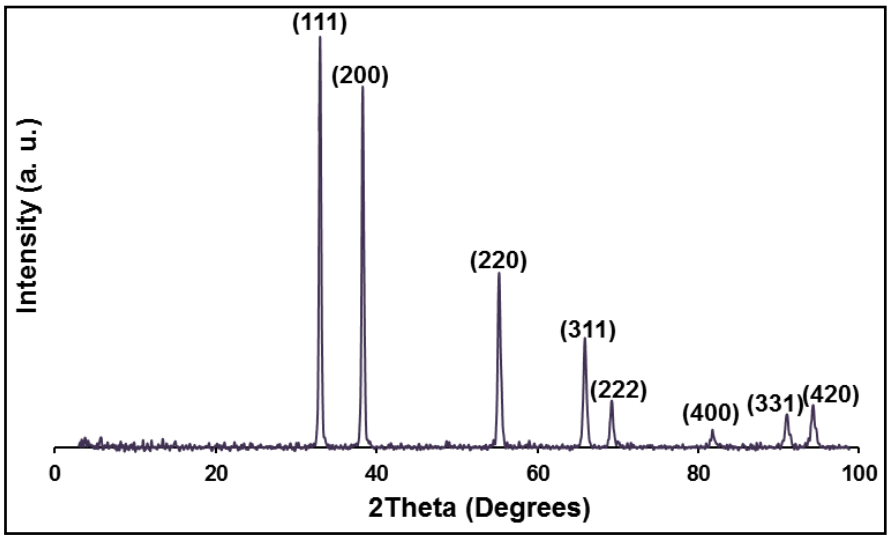

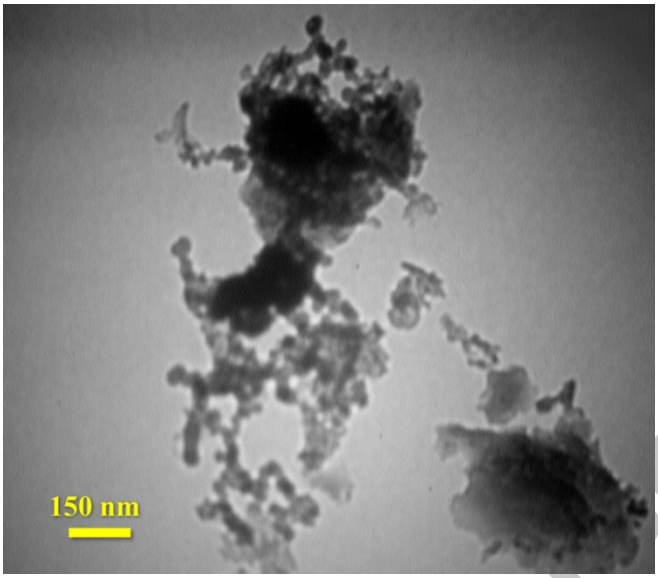

Fig. 14. The XRD pattern (up) and TEM image (down) of cadmium oxide nanoparticles obtained from calcination of cadmium iodide complex.

4. Conclusion

The sonochemical method was used for the synthesis of a new cadmium Schiff base complex. The structural data suggested a distorted square pyramidal geometry around cadmium center. In this geometry, the square base is formed by two iminic nitrogens (N1 and N2) from Schiff base ligand and two iodide anion (I1 and I2) while the apical position is occupied by aminic nitrogen (N3). FT-IR, NMR and XRD data are in agreement with the X-ray structure and confirm the phase purity of the prepared samples. The nanostructure nature of compound was approved by XRD and SEM techniques. The crystal packing analysis shows the inter-molecular interactions such as C–H···O, C–H···I and π···π interactions that cause the self-assembly process. These interactions are related to phenyl rings and their nitro substituents and also coordinated iodide anions. Hirshfeld surface analyses were carried out for the investigation of the nature and quantitative contributions of intermolecular interactions in the crystal packing. The surface mapped on d_{norm} function shows non-classical hydrogen bonds of C–H···O and C–H···I. Thermogravimetric analysis (TG/DTG) showed two thermal decomposition steps in the temperature range of 25 to 800 °C that finally left out the cadmium metal as final residue. A comparison between experimental and theoretical structure data represents similar geometries with slight structural discrepancies. Natural bond orbital (NBO) analysis and time-dependent density functional theory (TD-DFT) were performed for deeper study of structure and spectral aspects of the complex. Finally, the direct calcination of $CdLI_2$ complex was applied for preparation of cadmium oxide nanoparticles.

Acknoledgement. Partial support of this work by Yasouj University is appreciated.

References

[1] R. Sanyal, S.A. Cameron, S. Brooker, Synthesis and complexes of an N_4 Schiff-base macrocycle derived from 2,2′-iminobisbenzaldehyde, Dalton Trans. 40 (2011) 12277-12287.

[2] G. Brunet, F. Habib, I. Korobkov, M. Murugesu, Slow Magnetic Relaxation Observed in Dysprosium Compounds Containing Unsupported Near-Linear Hydroxo- and Fluoro-Bridges, Inorg.Chem. 54 (2015) 6195-6202.

[3] D. Visinescu, J. -P. Sutter, C. Ruiz-Perez, M. Andruh, A new synthetic route towards heterotrimetallic complexes. Synthesis, crystal structure and magnetic properties of a $[Cu^{II}Mn^{II}Cr^{III}]$ trinuclear complex, Inorg.Chim.Acta 359 (2006) 433–440.

[4] P. Sun, S. Liu, J. Han, Y. Shen, H. Sun, D. Jia, Solvothermal syntheses, crystal structures, and optical and thermal properties of transition metal selenidostannates, Transition Met.Chem. 42 (2017) 387-393.

[5] S. Kumar, R.P. Sharma, P. Venugopalan, V.S. Gondil, S. Chhibber, T. Aree, M. Witwicki, V. Ferretti, Hybrid inorganic-organic complexes: Synthesis, spectroscopic characterization, single crystal X-ray structure determination and antimicrobial activities of three copper(II)-diethylenetriamine-p-nitrobenzoate complexes, Inorg.Chim.Acta, 469 (2018) 288-297.

[6] F. -M. Wang, An Oxo-Bridged Dinuclear Vanadium(V) Complex of *N,N*′-bis(salicylidene)-1,5-diimino-3-azapentane: Synthesis and Structure, Synth.React.Inorg.,Met.-Org.,Nano-Met.Chem. 42 (2012) 1386-1389.

[7] H. Adams, D. E. Fenton, S. J.Ryan, Dicopper(I) and disilver(I) complexes of a thiophene-derived Schiff base macrocycle, inorg. chem. commun. 2 (1999) 52-54.

[8] B. N. Sarkar, S. Choubey, K. Bhar, S. Chattopadhyay, P. Mitra, B. K. Ghosh, Synthesis, structure and properties of hexacoordinated compounds of cadmium(II) halides/pseudohalides containing a pentadentate N-donor Schiff base, J.Mol.Struct. 994 (2011) 306–312.

[9] F.A. Cotton, G. Wilkinson, C.A. Murillo, M. Bochmann, Advanced Inorganic Chemistry, Sixth ed., John Wiley and Sons, New York, 1999.

[10] B. Naskar, R. Modak, D.K. Maiti, M.G.B. Drew, A. Bauza, A. Frontera, Ch. D. Mukhopadhyay, S. Mishra, K.D. Saha, S. Goswami, A Schiff base platform: structures,

sensing of Zn(II) and PPi in aqueous medium and anticancer activity, Dalton Trans. 46 (2017) 9498–9510.

[11] J. Chakraborty, S. Thakurta, B. Samanta, A. Ray, G. Pilet, S.R. Batten, P. Jensen, S. Mitra, Synthesis, characterisation and crystal structures of three trinuclear cadmium(II) complexes with multidentate Schiff base ligands, Polyhedron 26 (2007) 5139–5149.

[12] P. Abdolalian, A. Morsali, G. Bruno, Sonochemical synthesis and characterization of microrod to nanoparticle of new mixed ligand zinc(II) fumarate metal-organic polymer, Ultrason. Sonochem. 37 (2017) 654-659.

[13] H. Xu, B. W. Zeiger, K. S. Suslick, Sonochemical synthesis of nanomaterials, Chem. Soc. Rev. 42 (2013) 2555-2567.

[14] P. Hayati, A. R. Rezvani, A. Morsali, P. Retailleau, S. García-Granda, Influences of temperature, power ultrasound and reaction time on the morphological properties of two new mercury(II) coordination supramolecular compounds, Ultrason. Sonochem. 34 (2017) 968-977.

[15] M. Y. Masoomi, A. Morsali, P. C. Junk, J. Wang, Ultrasonic assisted synthesis of two new coordination polymers and their applications as precursors for preparation of nano-materials, Ultrason. Sonochem. 34 (2017) 984-992.

[16] M. Montazerozohori, A. Masoudiasl, Th. Doert, Two new 1D zigzag Hg(II) nanostructure coordination polymers: Sonochemical synthesis, thermal study, crystal structure and Hirshfeld surface analysis, Inorg.Chim.Acta 443 (2016) 207–217.

[17] Y. Hanifehpour, B. Mirtamizdoust, A. Morsali, S. W. Joo, Sonochemical syntheses of binuclear lead(II)-azido supramolecule with ligand 3,4,7,8-tetramethyl-1,10-phenanthroline as precursor for preparation of lead(II) oxide nanoparticles, Ultrason. Sonochem. 23 (2015) 275–281.

[18] M. J. Soltanian Fard, P. Hayati, A. Firoozadeh, J. Janczak, Ultrasonic Synthesis of two new Zinc(II) bipyridine Coordination Polymers: New Precursors for preparation of Zinc(II) Oxide nano-particles, Ultrason. Sonochem. 35 (2017) 502-513.

[19] K.S. Suslick, S.-B. Choe, A.A. Cichowlas, M.W. Grinstaff, Sonochemical synthesis of amorphous iron, Nature 353 (1991) 414–416.

[20] J.H. Bang, K.S. Suslick, Aplications of ultrasound to the synthesis of nanostructured materials, Adv. Mater. 22 (2010) 1039–1059.

[21] K. Ullah, Sh. Ye, S. -B. Jo, L. Zhu, K. -Y. Cho, W. -Ch. Oh, Optical and photocatalytic properties of novel heterogeneous $PtSe_2$–graphene/TiO_2 nanocomposites synthesized via ultrasonic assisted techniques, Ultrason. Sonochem. 21 (2014) 1849-1857.

[22] V. Safarifard, A. Morsali, Applications of ultrasound to the synthesis of nanoscale metal–organic coordination polymers, Coord. Chem. Rev. 292 (2015) 1–14.

[23] Zi Long, Meiying Liu, Ruming Jiang, Guangjiang Zeng, Qing Wan, Hongye Huang, Fengjie Deng, Yiqun Wan, Xiaoyong Zhang, Yen Wei, Ultrasonic-assisted Kabachnik-Fields reaction for rapid fabrication of AIE-active fluorescent organic nanoparticles, Ultrason. Sonochem. 35 (2017) 319–325.

[24] H. Kohler, Optical properties and energy-band structure of CdO, Solid State Commun 11 (1972) 1687–1690.

[25] F. Yakuphanoglu, Synthesis and electro-optic properties of nanosized-boron doped cadmium oxide thin films for solar cell applications, Sol. Energy 85 (2011) 2704–2709.

[26] F.A. Benko, F.P. Koffyberg, Quantum efficiency and optical transitions of CdO photoanodes, Solid State Commun. 57 (1986) 901-903.

[27] M. Soylu, H.S. Kader, Photodiode based on CdO thin films as electron transport layer, J. Elec Mater. 45 (2016) 5756-5763.

[28] R. Kondo, H. Okimura, Y. Sakai, Electrical properties of semiconductor photodiodes with semitransparent films, Jpn. J. Appl. Phys. 10 (1971) 1547-1550.

[29] M.M. Rahman, M.M. Alam, A.M. Asiri, M.A. Islam, Ethanol sensor development based on ternary-doped metal oxides (CdO/ZnO/Yb2O3) nanosheets for environmental safety, RSC Adv. 7 (2017) 22627-22639.

[30] M. Montazerozohori, S. Farokhiyani, A. Masoudiasl, J.M. White, Crystal structures, Hirshfeld surface analyses and thermal behavior of two new rare tetrahedral terminal zinc(II) azide and thiocyanate Schiff base complexes RSC Adv. 6 (2016) 23866-23878.

[31] M. Montazerozohori, A. Masoudiasl, S. Farokhiyani, Sh. Joohari, P. McArdle, Sonochemical synthesis of a new cobalt(II) complex: Crystal structure, thermal behavior, Hirshfeld surface analysis and its usage as precursor for preparation of CoO/Co_3O_4 nanoparticles, Ultrason. Sonochem. 38 (2017) 134–144.

[32] S. M. Jahromia, M. Montazerozohoria, A. Masoudiasl, E. Houshyar, S. Joohari, J.M. White, Sonochemical synthesis and characterization of new seven coordinated zinc, cadmium and mercury nitrate complexes: New precursors for nanostructure metal oxides, Ultrason. Sonochem. 41 (2018) 590–599.

[33] S.A. Mousavi, M. Montazerozohori, A. Masoudiasl, G. Mahmoudi, J.M. White, Sonication-assisted synthesis of a new cationic zinc nitrate complex with a tetradentate Schiff base ligand: Crystal structure, Hirshfeld surface analysis and investigation of different parameters influence on morphological properties, Ultrason. Sonochem. 46 (2018) 26–35.

[34] L. Taghizadeh, M. Montazerozohori, A. Masoudiasl, S. Joohari, J.M. White, New tetrahedral zinc halide Schiff base complexes: Synthesis, crystal structure, theoretical, 3D Hirshfeld surface analyses, antimicrobial and thermal studies, Mater. Sci. Eng. C 77 (2017) 229–244.

[35] G. M. Sheldrick, Crystal structure refinement with SHELXL, Acta Cryst. C 71 (2015) 3–8.

[36] C. F. Macrae, P. R. Edgington, P. McCabe, E. Pidcock, G. P. Shields, R. Taylor, M. Towler, J. van de Streek. Mercury: visualization and analysis of crystal structures, J. Appl. Crystallogr. 39 (2006) 453-457.

[37] O.V. Dolomanov, L.J. Bourhis, R.J. Gildea, J.A.K. Howard, H. Puschmann, OLEX2: a complete structure solution, refinement and analysis program, J. Appl. Cryst. 42 (2009) 339-341.

[38] M.A. Spackman, D. Jayatilaka, Hirshfeld surface analysis, CrystEngComm 11 (2009) 19-32.

[39] F.L. Hirshfeld, Bonded-atom fragments for describing molecular charge densities, Theor. Chim. Acta 44 (1977) 129-138.

[40] M.A. Spackman, J.J. McKinnon, Fingerprinting intermolecular interactions in molecular crystals, CrystEngComm 4 (2002) 378-392.

[41] A. Parkin, G. Barr, W. Dong, C.J. Gilmore, D. Jayatilaka, J.J. McKinnon, M.A. Spackman, C.C. Wilson, Comparing entire crystal structures: structural genetic fingerprinting, CrystEngComm 9 (2007) 648-652.

[42] S. K. Wolff, D. J. Grimwood, J. J. McKinnon, M. J. Turner, D. Jayatilaka, M. A. Spackman, CrystalExplorer, University of Western Australia, 2012.

[43] M. J. Frisch et al., Gaussian 03, Revision C02, Gaussian Inc, Wallingford CT, 2004.

[44] C. Lee, W. Yang, R. G. Parr, Development of the Colle-Salvetti correlation-energy formula into a functional of the electron density, Phys. Rev. B17 (1988) 785–789.

[45] G. Keresztury, S. Holly, J. Varga, G. Besenyei, A.Y. Wang, J.R. Durig, Vibrational spectra of monothiocarbamates-II. IR and Raman spectra, vibrational assignment, conformational analysis and *ab initio* calculations of *S*-methyl-*N,N*-dimethylthiocarbamate Spectrochim. Acta A 49 (1993) 2007–2026.

[46] E. D. Glendening, A. E. Reed, J. E. Carpenter, F. Weinhold, NBO Version 3.1, TCI, University of Wisconsin, Madison, 1998.

[47] E. Gross, W. Kohn, Time-Dependent Density-Functional Theory, Adv. Quant. Chem. 21 (1990) 255-291.

[48] Y. W. Zhang, S. Jin, S. J. Tian, G. B. Li, T. Jia, C. S. Liao, C. H. Yan, Sol-Gel Fabrication and Electrical Property of Nanocrystalline $(RE_2O_3)_{0.08}(ZrO_2)_{0.92}$ (RE) Sc, Y) Thin Films, Chem. Mater. 13 (2001) 372-378.

[49] A. Masoudiasl, M. Montazerozohori, R. Naghiha, A. Assoud, P. McArdle, M. Safi Shalamzari, Synthesis, X-ray crystal structures and thermal analyses of some new antimicrobial zinc complexes: new configurations and nano-size structures, Mater. Sci. Eng. C 61 (2016) 809-823.

[50] K. Nakamoto, Infrared and Raman Spectra of Inorganic and Coordination Compounds, Part B, fifth ed. Wiley, New York, 1997. 116.

[51] M. Montazerozohori, A. Nazaripour, A. Masoudiasl, R. Naghiha, M. Dusek, M. Kucerakova, Antimicrobial activity, DNA cleavage, thermal analysis data and crystal structure of some new $CdLX_2$ complexes: a supramolecular network, Mater. Sci. Eng. C 55 (2015) 462-470.

[52] M. Montazerozohori, Z. Khadem, A. Masoudiasl, R. Naghiha, S. Ghanbari, Th. Doert, A zinc iodide complex with two-dimensional supra-molecular network: new antimicrobial four coordinated zinc complexes, J. Iran. Chem. Soc. 13 (2016) 779–791.

[53] A.W. Addision, T.N. Rao, J. Reedijik, J.V. Rijn, G.C. Verschoor, Synthesis, structure, and spectroscopic properties of copper (II) compounds containing nitrogen**s**ulphur donor ligands; the crystal and molecular structure of aqua [1, 7-bis (N-methylbenzimidazol-2*0*-yl)-2, 6-dithiaheptane] copper (II) perchlorate, J. Chem. Soc. Dalton Trans. (1984) 1349**-**1356.

[54] M. Montazerozohori, A. Masoudiasl, Th. Doert, H. Seykens, Structural and computational study of some new nano-structured Hg(II) compounds: a combined X-ray, Hirshfeld surface and NBO analyses, RSC Adv. 6 (2016) 21396–21412.

[55] S. Ghanbari Niyaky, M. Montazerozohori, A. Masoudiasl, J.M. White, New five coordinated supramolecular structured cadmium complex as precursor for CdO nanoparticles: Synthesis, crystal structure, theoretical and 3D Hirshfeld surface analyses, J. Mol. Struct. 1131 (2017) 201–211.

[56] S.H. Rahaman, R. Ghosh, G. Mostafa, B.K. Ghosh, Unusual perchlorate binding in heptacoordinated cadmium(II) thiocyanate containing a pentadentate Schiff base Inorg.Chem.Commun. **8** (2005) 700-703.

[57] M.G.B. Drew, S. Hollis, The structure of diiodo{*S*,*S*'-dimethyl-2,6-bis[1-(2-thio-phenylimino)ethyl]pyridine}cadmium(II),ActaCrystallogr.,Sect.B:Struct.Crystallogr.Cryst.Chem. 34 (1978) 2853-2856.

[58] D. Li, Q. Zhang, P. Wang, J. Wu, Y. Kan, Y. Tian, H. Zhou, J. Yang, X. Tao, M. Jiang, Studies of the isomerization and photophysical properties of a novel 2,2′:6′,2″-terpyridine-based ligand and its complexes, Dalton Trans. 40 (2011) 8170-8178.

[59] C. Janiak, A critical account on π-π stacking in metal complexes with aromatic nitrogen-containing ligands, J. Chem. Soc. Dalton Trans. (2000) 3885-3896.

[60] S. Grabowsky, P.M. Dean, B.W. Skelton, A.N. Sobolev, M.A. Spackman, A.H. White, Crystal packing in the 2-R,4-oxo-[1,3-*a*/*b*]-naphthodioxanes – Hirshfeld surface analysis and melting point correlation, CrystEngComm 14 (2012) 1083-1093.

[61] S.A. Zarei, K. Akhtari, K. Hassanzadeh, M. Piltan, S. Saaidpour, M. Abedi, Halide (Cl^-, Br^-, I^-) influence on the electronic properties of macrocyclic nickel(II) complexes: ab-initio DFT study, J. Korean Chem. Soc. 57 (2013) 311-315.

[62] M. Montazerozohori, S. A. Musavi, A. Masoudiasl, A. Naghiha, M. Dusek, M. Kucerakova, Synthesis, spectral, crystal structure, thermal behavior, antimicrobial and DNA cleavage potential of two octahedral cadmium complexes: A supramolecular structure, Spectrochim. Acta A, 137 (2015) 389–396.

[63] S.A. Musavi, M. Montazerozohori, A. Masoudiasl, R. Naghiha, S. Joohari, A. Assoud, Crystal structure, DNA interaction and thermal analysis data of two new antimicrobial active binuclear cadmium and mercury complexes, J. Mol. Struct. 1145 (2017) 65-75.

[64] F. Weinhold, C.R. Landis, Natural bond orbitals and extensions of localized bonding concepts, Chem. Educat. Resear. Pract. 2 (2001) 91-104.

Highlights

►A new nanostructured cadmium coordination compound was prepared.

►The crystal packing was contained C–H···O, C–H···I and π···π interactions.

► Hirshfeld surfaces and corresponding fingerprint plots of the complex were evaluated.